WPMST1-PR(18) 20879

MCC Messmer et al.

Optimal MSE polarisation angle and q-profile estimation using Kalman Filters and the plasma simulator RAPTOR

Preprint of Paper to be submitted for publication in
Plasma Physics and Controlled Fusion

This work has been carried out within the framework of the EUROfusion Consortium and has received funding from the Euratom research and training programme 2014-2018 under grant agreement No 633053. The views and opinions expressed herein do not necessarily reflect those of the European Commission.

Optimal MSE polarisation angle and q-profile estimation using Kalman Filters and the plasma simulator RAPTOR

Messmer M.C.C.[1], Felici F. [1], Loenen J.P.G.[1], Sauter, O.[2], Teplukhina, A.A.[2], Reich M.[3], Fischer R.[3], Rittich D.[3], Jaspers R.J.E.[1,4], the ASDEX Upgrade Team and the EUROfusion MST1 team[5]

[1]Eindhoven University of Technology (TU/e), 5600MB Eindhoven, The Netherlands.
E-mail: m.c.c.messmer@tue.nl
[2]École Polytechnique Fédérale de Lausanne (EPFL), Centre de Recherches en Physique des Plasmas, Association EURATOM-Suisse, 1015 Lausanne, Switzerland
[3]Max-Planck-Institut für Plasmaphysik, Boltzmannstr. 2, 85748 Garching, Germany
[4]Department of Applied Physics, Ghent University, 9000 Ghent, Belgium
[5]See the author list of H. Meyer et al 2017 Nucl. Fusion 57 102014

July 3, 2018

Abstract

Accurate q-profile reconstruction is of importance for the development of advanced scenarios, but continues to be a challenge in tokamak research. To constrain the q-profile in the plasma centre the Motional Stark Effect diagnostic (MSE) is often used, however achieving routine measurements with the required accuracy proves to be difficult in many devices. We present a novel approach to obtain accurate estimates of the q-profile using an observer based approach. The observer combines MSE measurements with model based prediction of the system. For this the plasma transport simulator RAPTOR [1] is coupled with a fixed boundary equilibrium solver to create a model based prediction of the MSE measurements. An Extended Kalman Filter (EKF) is used to merge profile evolution predictions from the RAPTOR code with measurements. Using synthetic data we demonstrate accurate q-profile estimations in situations where the model is purposely disturbed and only erroneous MSE measurements are available. For shots at ASDEX Upgrade we show that by constraining RAPTOR with MSE measurements, the evolution of the model's q-profile is in close proximity to reference profiles of reconstructed equilibria from an integrated diagnostic suite.

1 Introduction

Of the available concepts for nuclear fusion reactors, the most matured one is the Tokamak. It confines the plasma by a helical magnetic field which is created by external coils and a current running through the plasma. The externally applied toroidal component of the magnetic field is known, however the field components generated by the plasma current are difficult to measure and manipulate. Tailoring the plasma's current density profile J, or its derived quantity, the q-factor $q = d\Phi/d\psi$, where Φ is the toroidal magnetic flux, and ψ the poloidal magnetic flux, is essential for plasma stability and performance [2].

Unfortunately, no direct measurement of q (or J) is available. The plasma equilibrium, specifically the distribution of poloidal flux ψ(R,Z) and the free functions $p'(\psi)$, $FF'(\psi)$, are estimated using (real-time) equilibrium reconstruction codes that solve the 2D Grad-Shafranov equation, a two-dimensional, nonlinear, elliptic partial differential equation describing the force balance in the plasma [3, 4]. This process usually involves parametrising the internal profiles and solving a least-square problem constrained by internal and external measurements of the plasma. External measurements are magnetic probes, flux loops and Rogowski coils, internal measurements are for example temperature and density measurements. By using magnetic probes, the plasma equilibrium can be reconstructed with good accuracy at the plasma boundary, however in order to constrain the internal current distribution, knowledge of the internal magnetic field is required. In the plasma centre, Grad-Shafranov solvers are typically constrained by measurements from the Motional Stark Effect (MSE) diagnostic [5] or polarimetric measurements [6]. MSE systems locally measure the magnetic pitch angle, the angle between the toroidal field B_ϕ and the poloidal field B_θ. A continuous challenge of the MSE diagnostic is to record data with sufficient accuracy for a good q-profile reconstruction. For a precise reconstruction, for example to accurately resolve the evolution of the central safety factor during sawtooth events, a measurement accuracy of 0.1° on a millisecond timescale is required [7, 8].

In this article we propose a novel way to use a model-based observer to obtain accurate estimates of the magnetic pitch angles. This approach results in higher quality estimates than can be achieved by using only measurement or model data and can also complement situations where direct measurements from MSE are not available, or are not sufficiently accurate. The observer combines MSE measurements with model based prediction of the system for better estimates of the state of

the system. This provides:

- a check of the measurement quality (or the simulation quality),
- better estimates of the state of the model by combining the real and predicted measurement,
- a real-time capable filtering solution,
- a constrain on the q-profile by the model in cases where MSE data is not available,
- a correction of the model in case of model mismatch.

As a physics model describing the process, we use the poloidal flux diffusion equation and electron transport equation [9], implemented in the RAPTOR code [1].

A recently developed approach, similar to the one described in this paper, is implemented in the IDE code [10, 11]. In this approach, a Bayesian approach is used to merge diagnostic measurements related to the core current density with a one-step-ahead prediction based on the poloidal flux diffusion equation. Important differences between both approaches are that RAPTOR is capable to run in real-time and the physics model in IDE only includes the poloidal flux diffusion equation, while the kinetic core profiles are obtained from a Bayesian reconstruction using several diagnostics for individual time slices. The approach of combining RAPTOR with an Extended Kalman Filter contains a predictive model for the electron temperature (with future versions including also ion temperature and particle transport equations [12]), allowing the EKF approach to be applied to reconstruct all the core profiles. At the same time, it is important to realise the similarities between the Bayesian approach of IDE and the Kalman Filter approach in this paper. Indeed, it can be shown that the Kalman Filter can be written as a special case of a Bayesian estimator assuming the noise is Gaussian. The great advantage of Kalman Filter above more general Bayesian reconstruction is its speed, which allows real-time implementation. In previous work [13], RAPTOR has been used on TCV, AUG and RFX to estimate the core electron temperature and q-profile, constrained by measurements of core density and temperature.

In this work, we show for the first time that RAPTOR can be constrained by MSE measurements to accurately model the q-profile evolution. A prediction of the polarisation angle γ is not possible from the state of the model (RAPTOR) alone, but requires knowledge of the 2D magnetic field structure. To be able to calculate γ, RAPTOR has been coupled to a Grad-Shafranov solver

(CHEASE [14]) in a self consistent way, which ensures that the geometry-dependent terms that enter the current diffusion equation (CDE) evolve consistently with the 2D equilibrium, and at the same time the equilibrium is correctly constrained by the q-profile from the CDE. This coupling allows a fast and accurate calculation of current density profile given by the CDE from the state in combination with the plasma equilibrium.
In the future we want to couple RAPTOR to a real-time capable equilibrium solver for real-time q-profile prediction and control. Then, instead of constraining the GS solver by RAPTOR's q-profile, the filtered polarisation angle would be used as a constrain to ensure consistent q-profiles between RAPTOR and the equilibrium solver.

The remainder of this article is structured as follows:
Section 2 provides an introduction to the EKF, followed by a description of the RAPTOR code and a brief outline of the MSE diagnostic and the difficulties present at the ASDEX Upgrade Tokamak. In section 3 the EKF is first tested on a virtual MSE diagnostic, where γ is calculated from the model, and lastly the EKF is used to constrain RAPTOR's q-profile with MSE measurements from ASDEX Upgrade. The conclusions are presented in section 4.

2 Methology

2.1 Extended Kalman Filter

To provide the best estimate of the state of a system, an Extended Kalman Filter (EKF) can be used to filter real measurements with model predicted measurements of the system. The EKF, the non-linear extension of the Kalman Filter (which is used for systems described by linear ODE's), has been described in literature extensively [15]. The EKF has the advantage that it not only takes the measurement and model into account, but it is also recursive, fast and can handle asynchronous measurements. Only the main concepts of the EKF algorithm are outlined here, the interested reader is refered to [15, 16] for a more detailed description.
The EKF algorithm is illustrated in figure 2.1. For every time step k, the EKF algorithm consists of 4 steps. Our notation follows the one of Simon [15], the hat denotes a predicted quantity from the model and the subset, e.g. $k|k-1$, denotes that the quantity is evaluated for time k, taking into account the history of the quantity up to time $k-1$.

Step 1: The EKF uses a model of the system in the form of a nonlinear ODE $x_k = f(x_{k-1}, u_{k-1}, w_{k-1})$, where x_k describes the state of the system, u are inputs to the model and w is the noise vector of the state. First, the partial derivatives of the model function are calculated

$$F_{k-1} = \left.\frac{\partial f_{k-1}}{\partial x}\right|_{\hat{x}_{k-1}}, \tag{2.1}$$

$$G_{k-1} = \left.\frac{\partial f_{k-1}}{\partial w}\right|_{\hat{x}_{k-1}}. \tag{2.2}$$

$$\tag{2.3}$$

Step 2: Predict the state estimate and estimation-error covariance matrix:

$$\hat{x}_{k|k-1} = f(\hat{x}_{k-1}, u_{k-1}, 0), \tag{2.4}$$

$$\Sigma_{k|k-1} = F_{k-1}\Sigma_{k-1}F_{k-1}^T + G_{k-1}Q_{k-1}G_{k-1}^T. \tag{2.5}$$

Here, Σ is the estimation-error covariance matrix and Q_k is the covariance matrix of the model.

Step 3: Calculate the partial derivatives of the predicted measurement function $\hat{y}_k = h(\hat{x}_k, v)$:

$$H_k = \left.\frac{\partial h_k}{\partial x}\right|_{\hat{x}_{k|k-1}}, \tag{2.6}$$

$$M_k = \left.\frac{\partial h_k}{\partial v}\right|_{\hat{x}_{k|k-1}}, \tag{2.7}$$

with v being the noise vector of the measurement.

Step 4: Update the state and error covariance estimate:

$$L_k = \Sigma_{k|k-1} H_k^T \left(H_k \Sigma_{k|k-1} H_k^T + M_k R_k M_k^T\right)^{-1}, \tag{2.8}$$

$$\hat{x}_{k|k} = \hat{x}_{k|k-1} + L_k \left(y_k - h_k(\hat{x}_{k|k-1})\right), \tag{2.9}$$

$$\Sigma_{k|k} = (I - L_k H_k)\, \Sigma_{k|k-1}, \tag{2.10}$$

where y_k is a real measurement of the system.
For a smooth initialisation of the EKF, the Kalman gain is multiplied with a time dependent function:

$$L'_k = L_k \cdot \exp\left(-0.12 \cdot (t - t_0)\right), \tag{2.11}$$

where t_0 is the first active time step of the observer and the factor 0.12 was arbitrarily chosen.

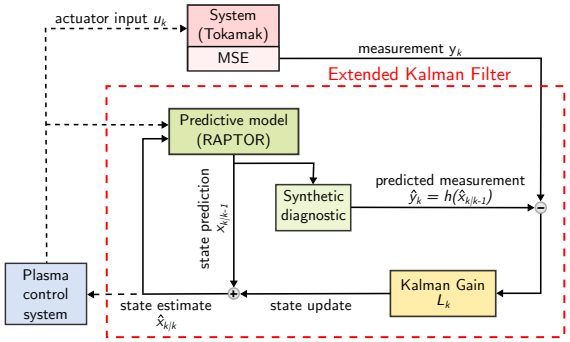

Figure 2.1: Overview of the Extended Kalman Filter: The predictive model (RAPTOR) simulates the state of the system from which the measurement (polarisation angles) can be predicted. In combination with the real measurement the EKF updates the state to obtain an improved estimate.

The system is described by the current diffusion equation and heat transport equations, implemented by the transport simulator RAPTOR. The state of the model $\hat{x}$ is a representation of the poloidal flux ψ and the electron temperature T_e, from which various plasma parameters - for this article most importantly the safety factor q - can be derived. As measurements, the polarisation angle measurements from the MSE diagnostic y_k are taken. The model, measurement and measurement prediction, will be explained in the following sections.

A central quantity for the EKF algorithm are the noise of the state and measurement, w_k and v_k respectively, from whose covariance matrices the Kalman Gain is calculated (equation 2.8). The covariance matrices are essential for the performance and tuning of the EKF. They determine the weighting of the model, or measurement, and are used to tune the performance of the EKF.
The process covariance matrix Q_k of the model has previously been defined in [16]. It is designed to enforce a high correlation between neighbouring spatial points based on physical and numerical consideration of the problem.
The covariance matrix of the measurement is a diagonal matrix containing the square of the standard deviation of each measurement channel as diagonal entries. It is described in more detail in section 2.3.

2.2 Plasma evolution model: RAPTOR

The observer is based on a model of the system (the tokamak), which provides estimates of the state of the system from which the expected measurement can be derived. The system is modelled by the transport simulator RAPTOR. This fast real-time capable code solves the coupled 1D poloidal flux (ψ), electron- and ion- temperature (T_e, T_i) equations, as well as particle transport equations for electrons and multiple ion species [12]. For the present work, we solve only the equations for ψ (equation 2.12) and T_e (equation 2.13).

$$\sigma_{||}\left(\left.\frac{\partial\psi}{\partial t}\right|_{\hat{\rho}} - \frac{\hat{\rho}\dot{\Phi}_b}{2\Phi_b}\frac{\partial\psi}{\partial\hat{\rho}}\right) = \frac{F^2}{16\pi^2\mu_0\Phi_b^2\hat{\rho}}\frac{\partial}{\partial\hat{\rho}}\left[\frac{g_2 g_3}{\hat{\rho}}\frac{\partial\psi}{\partial\hat{\rho}}\right] - \frac{B_0}{2\Phi_b\hat{\rho}}V'_{\hat{\rho}}\left(j_{\text{aux}} + j_{\text{bs}}\right) \tag{2.12}$$

In equation 2.12, $\sigma_{||}$ is the neoclassical conductivity, j_{aux} is the non-inductive driven current by auxiliary systems, j_{bs} the bootstrap current, and g_2, g_3, F, $V'_{\hat{\rho}}$ define the geometry of the simulation and are calculated from magnetic equilibria.
The electron energy transport equation is written as:

$$\begin{aligned}\frac{3}{2}\left(V'_{\hat{\rho}}\right)^{-5/3}\left(\left.\frac{\partial}{\partial t}\right|_{\hat{\rho}} - \frac{\dot{\Phi}_b}{2\Phi_b}\frac{\partial}{\partial\hat{\rho}}\hat{\rho}\right) + \\ \left[\left(V'_{\hat{\rho}}\right)^{5/3} n_e T_e\right] + \frac{1}{V'_{\hat{\rho}}}\frac{\partial}{\partial\hat{\rho}}\left(-\frac{g_1}{V'_{\hat{\rho}}}n_e\chi_e\frac{T_e}{\partial\hat{\rho}} + \frac{5}{2}T_s\Gamma_e g_0\right) = P_s\end{aligned} \tag{2.13}$$

With electron temperature, density, thermal diffusivity, convective flux T_e, n_e, χ_e, Γ_e and geometric terms g_0, g_1. P_s denotes the sum of the power density sources and sinks. $\dot{\Phi}_b$, $\hat{\rho}$ and B_0 are the toroidal flux enclosed by the LCFS, the normalised square root of the toroidal flux and toroidal magnetic field at the magnetic axis, respectively.
Equation 2.12 and 2.13 follow the notation introduced in [12], where a detailed description of the individual terms is provided.

The equations are solved on a radial grid corresponding to the normalised toroidal flux and are depending on the plasma and flux surface shape.
The thermal transport coefficients χ_e is provided by a gradient based empirical transport model [17] with free parameters tuned to match profiles calculated by the IDE code. The equilibrium calculated by IDE is taken as reference for this analysis. The particle flux term Γ_e in the temper-

ature equation is neglected in this work. The code has been used for simulation of TCV and AUG plasmas [17], JET [12] and ITER [18].

2.3 MSE diagnostic

Equilibrium solvers reconstruct the magnetic equilibrium in the plasma by solving the Grad-Shafranov equation, constrained by various measurements. As a constraint in the plasma centre, the MSE diagnostic is commonly used which provides a measure for the local magnetic pitch angle, the angle between B_ϕ and B_θ at a specific point in the plasma. The Motional Stark Effect (short MSE) diagnostic measures the light emitted by neutral particles, which are injected into the plasma. Typically the radiation of the particles injected by the neutral beam injectors used for heating, current drive and fuelling of the plasma is analysed. Due to the Stark effect the emitted light is polarised relative to the magnetic field; measurements of the polarisation angle can be linked to the pitch angle of the magnetic field projected in a plane perpendicular to the diagnostic's line of sight [5]. The MSE diagnostic at AUG can measure the polarisation angles at 8 different radial positions, with up to two channels per radius. The diagnostic measures the radiation of the Balmer-α line, which, due to the Stark effect, is degenerate into a total of 9 lines with different polarisations. The lines can be grouped in two categories: π- and σ-lines, which are polarised perpendicular and parallel to the electric field vector. The setup at AUG allows simultaneous measurement of both spectral components at similar radial and vertical positions [19–21].

The configuration of the MSE channels for the shots analysed in this article is shown in figure 2.2. 6 channels of the diagnostic are configured to record the σ lines of the stark spectrum and 2 the π emission. The measurement location of the π channels are in proximity to the σ channels. In a shot with high quality MSE data, the relationship $\sigma_n \approx \pi_n - 90^\circ$ holds, where $n = 1, 2$ refers to one of the two channel pairs marked in purple in figure 2.2.

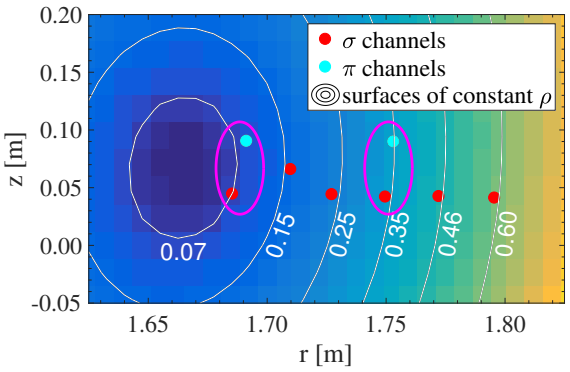

Figure 2.2: Poloidal plane, CHEASE flux surfaces and corresponding toroidal ρ values. Plotted are the spatial locations of the MSE channels and contour lines of constant ρ intersecting the MSE channels. Note that the values of ρ are subject to change during the shot, shown is the reconstructed grid for $t = 3.7$ s, shot *#33134*. The q-profile can not be constrained by MSE signals in the vicinity of the plasma edge. No MSE channels are available here, however q_{95} is constrained by the total plasma current.

A challenge at AUG is the contamination of the recorded signal with background polarised light, originating from reflections on the inner metallic wall of the device [21]. This background polarised light renders the recorded signals useless in high density discharges. One extreme example of a contaminated measurements is shown in figure 2.3: The diagnostic was configured to record five $\pi - \sigma$ measurement pairs simultaneously, which should display a 90° difference. During the shot, this can only been observed within the first 1.7 s of the shot after which the density is increased and the lines begin to diverge [21], rendering the measurement useless.

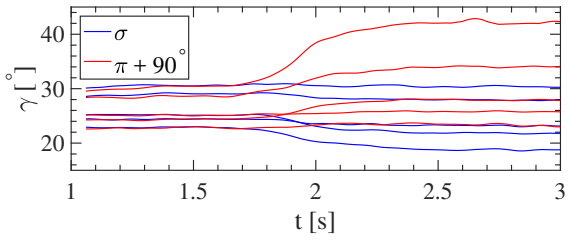

Figure 2.3: Example of the high-noise contaminated MSE measurements, recorded in AUG shot *#31313* (adapted from [21]).

Similar problems have been reported at Alcator C-Mod, where as a solution the MSE polychromator has been developed [22]. The MSE polychromator measures the $\pi + \sigma$ emission as well as the background polarisation in wavebands close to the measurement wavelengths for every channel.

The polarisation angles are than corrected by subtraction of the background.

The simultaneous measurement of π and σ lines is used to derive a time-varying estimate of the variance of each MSE measurement: The measurement covariance matrix R_k, required by the EKF (equation 2.8), is calculated from the two available $\pi - \sigma$ pairs (see figure 2.2) by calculating their time averaged difference:

$$\Delta\gamma(t) = \frac{1}{2}\sum_{n=1}^{2} \overline{\left|\left(\gamma_n^{\sigma} - (\gamma_n^{\pi} - 90°)\right)\right|} \tag{2.14}$$

$$\equiv \frac{1}{2}\overline{\Delta\Gamma}, \tag{2.15}$$

where the overbar denotes that for each time t, $\Delta\Gamma$ is averaged over the previous 20 ms. The diagonal elements of the covariance matrix, corresponding to the covariances of the individual MSE channels, are then $R_k = (\Delta\gamma)^2$.

2.4 Measurement prediction

The EKF requires the calculations of the predicted measurement from the model. The polarisation angle is calculated by

$$\gamma = \tan^{-1}\left(\frac{a_0 B_z + a_1 B_r + a_2 B_\phi}{a_3 B_z + a_4 B_r + a_5 B_\phi}\right), \tag{2.16}$$

where the a_i are known device specific geometric coefficients, that depend on the setup of the MSE diagnostic. $B_z(r,z)$ and $B_r(r,z)$ are the vertical and radial components of the poloidal magnetic field B_θ, and $B_\phi(r,z)$ is the toroidal magnetic field at the measurement point r, z. Note that equation 2.16 is a reduced form which neglects contributions from electric fields, which can lead to high uncertainties in advanced plasma scenarios [23]. The radial electric fields can not be obtained from RAPTOR. For improved accuracy E_r must be estimated from ion pressure profiles and toroidal and poloidal velocities [24].

From equation 2.16 it is clear that γ can not be derived from the RAPTOR state alone, since RAPTOR calculates 1D profiles and does not reconstruct the 2D equilibrium. The plasma equilib-

rium, constrained by RAPTOR's q-profile, must be calculated in order to calculate the predicted measurement. Then, by rewriting the poloidal magnetic field as

$$B_\theta = e_\phi \times (2\pi R)^{-1} q^{-1} \nabla \Phi, \tag{2.17}$$

the polarisation angle can be calculated by using $\Phi = \Phi_{\mathrm{EQ}}$ (i.e. the toroidal flux is obtained from the plasma equilibrium) and $q = q_{\mathrm{RAPTOR}}$.

2.5 Coupling between RAPTOR and CHEASE

The RAPTOR code does not evolve the plasma geometry, but instead assumes it to be fixed throughout the simulation. A time dependent coupling between RAPTOR and an equilibrium reconstruction code is required to calculate the spatial distribution of magnetic fields required to estimate gamma locally. This requires to constrain an equilibrium solver with RAPTOR's q-profile and updating geometry terms in the transport equation from the equilibrium before continuing the iteration of the transport equations. In practice this can be achieved by constraining both codes with the same MSE angles. Also, the flux surface shape as well as Φ changes slowly compared to *psi* and thus q. Updates of the plasma equilibrium are not required with every iteration of the CDE, allowing for an asynchronous coupling between RAPTOR and the Grad-Shafranov solver.
For the presented analysis, RAPTOR has been coupled to CHEASE [14], a fixed-boundary equilibrium solver, which solves the GS equation using specified boundary conditions and internal profiles. The last-closed flux surface and magnetic fields are used as inputs by CHEASE and are directly provided by RAPTOR. The pressure profile in terms of normalized toroidal flux $p(\hat{\rho}_\Phi)$, with $\hat{\rho}_\Phi = \sqrt{\Phi/\Phi_{\mathrm{edge}}}$, can also be used as input profile. The use of $\hat{\rho}_\Phi$ allows a direct coupling with RAPTOR, since it is RAPTOR's radial coordinate, and is less sensitive to changes in the q-profiles. This requires CHEASE to transform internally to profiles with respect to the poloidal flux, a solution of the GS equation. Another new option has recently been introduced in CHEASE, namely to provide the $q(\hat{\rho}_\Phi)$ profile as input [25]. In this case CHEASE computes the current density profile I^*, related to j_ϕ, such as to match the input q-profile and iterates until convergence. This usually leads to a finite current density at the plasma boundary which can be reduced by slightly modifying the radial derivative of q near the edge. CHEASE can use the previous equilibrium as initial guess which accelerates significantly the present coupling with RAPTOR.

The implementation allows dynamic updates of the geometry at arbitrary time steps of the simulation; it is illustrated in figure 2.4. The implemented coupling calculates the plasma equilibrium based on RAPTOR's q- and pressure profiles every n-th RAPTOR iteration [1]. From the equilibrium, the geometry, i.e. the shape of the poloidal flux surfaces as well as the toroidal flux they enclose (in detail terms g_1, g_2, g_3, V' and F in equation 2.12, 2.13) are calculated before the iteration of the transport equations is continued. This asynchronous implementation allows for a fast and accurate calculation of the polarisation angle, which can be used in offline and real-time simulations alike.

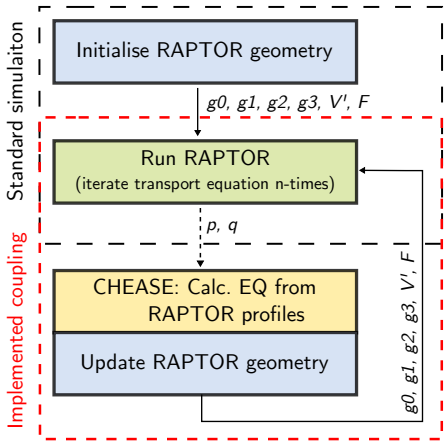

Figure 2.4: Flow diagram of the implemented coupling between RAPTOR and CHEASE.

The importance of the equilibrium update shows figure 2.5. Here, RAPTOR was run twice with identical simulation parameters, however, in one case the geometry was prescribed and fixed throughout the simulation (based on equilibria previously calculated by IDE), and in the second case the geometry terms were updated during the simulation.
Without the implemented coupling, the geometry is always calculated from previously reconstructed equilibria, which are estimated to match the currently simulated shot. The resulting uncertainties are unacceptable for a sensible calculation of γ.

[1] Technically CHEASE was constraint by the parallel current density $j_{||}$ and p, which is computational easier and available from RAPTOR. We verified that constraining $j_{||}$ or q results in similar results.

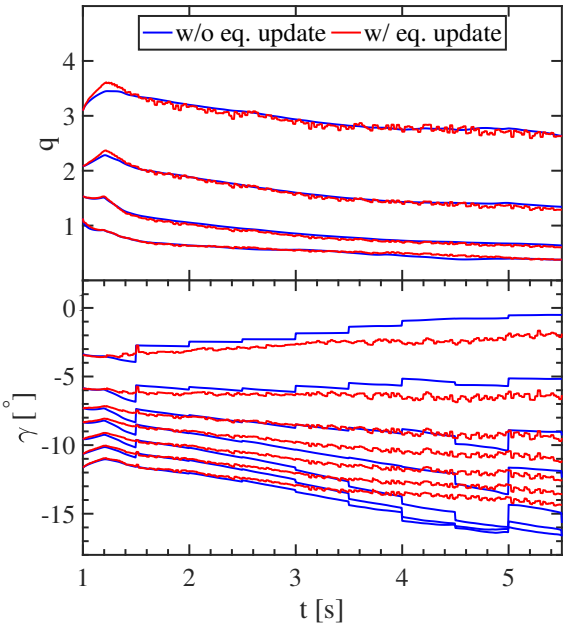

Figure 2.5: RAPTOR simulations with and without equilibrium update: Top: q values. Bottom: calculated γ. No simulation parameters where changed resulting in the equal evolution of q. The a priori calculated geometry (—) is based on equilibria from IDE which were loaded in half-second intervals. This is manifested in step-wise changes in γ. In the coupled simulation (—) the geometry is updated every 5th simulation step.

3 Implementation of the MSE observer

3.1 EKF tuning using synthetic data

The MSE observer is implemented and the performance is evaluated with synthetic data. The aim is to test and validate the implementation and investigate the effect of various settings of the EKF. For this, artificial MSE measurements are generated by simulating an AUG shot with RAPTOR, used in purely predictive mode as in [17]. Matching plasma equilibria are calculated with CHEASE. From the simulation result and equilibria the expected MSE polarisation angles are calculated as described in section 2.4 and 2.5. This simulation and synthetic diagnostic are assumed to correspond to the true evolution of the plasma profiles (q, T_e, ...) and corresponding true measurements, i.e. the nominal case.

A uniformly distributed random noise with standard deviation of $\Delta\gamma = 0.5^\circ$ is added to the polarisation angles to simulate the effect of measurement noise. This noise level is arbitrarily chosen and approximately 5 times higher than the acceptable error margins on MSE signals. Furthermore, the model used by the EKF is perturbed with respect to the nominal simulation. Firstly, the q-profile used to initialise the simulation at t = 0 is elevated, see figure 3.1 (d), 3.2 at t = 0. Additionally, the electron temperature transport coefficient is reduced by 30%, which yields a higher temperature, higher conductivity and correspondingly different q-profile evolution.

The input to the EKF are the perturbed simulation and noisy polarisation angles. The q-profile is evaluated to verify that the EKF is able to provide a good estimate of the q-profile matching the nominal case.

The time evolution of various quantities of the nominal and observer simulation are shown in figure 3.1. The model mismatch due to the reduced transport is clearly visible in the central electron temperature evolution in figure 3.1 c). For the observer case, the initially perturbed q-profile, figure 3.1 d), converges within ≈ 80 ms to the q-profile of the nominal simulation, only a slight mismatch is visible at the q values towards the plasma centre, which is the most affected by the reduced heat transport.

The innovation sequence $\mathfrak{I} = z_k - h(\hat{x}_{k|k-1})$, the difference between measured and model predicted MSE data, shown in fig. 3.2 e), is expected to be zero mean if the underlying system is linear. For the non-linear case it still serves as an indication on the performance of the EKF. In the analysed scenario $\mathfrak{I}$ does not converge to a zero mean, but stays close to zero. This implies that a constant correction from the observer on the q-profile is required. Contradictory to [16], no disturbance estimation is required due to the relatively large timescales of the current diffusion time.

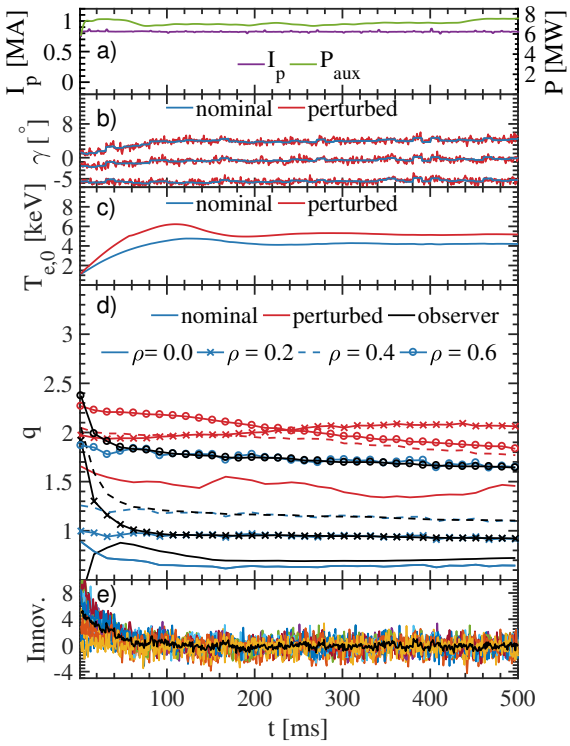

Figure 3.1: Summary of the MSE observer results using synthetic MSE data (based on AUG shot *#33134*). a) Plasma current and aux. power. b) calculated polarisation angle without (—) and with 0.5° noise (—). c) central electron temperature of the nominal and perturbed simulation. d) comparison of the q-value evolution at $\rho = 0, 0.2, 0.4, 0.6$ between the nominal simulation, perturbed simulation and MSE observer. e) Innovation sequence, the difference between measured and model predicted MSE data.

The q-profile of the nominal and perturbed simulation as well as the observer results are compared for various time steps in figure 3.2.

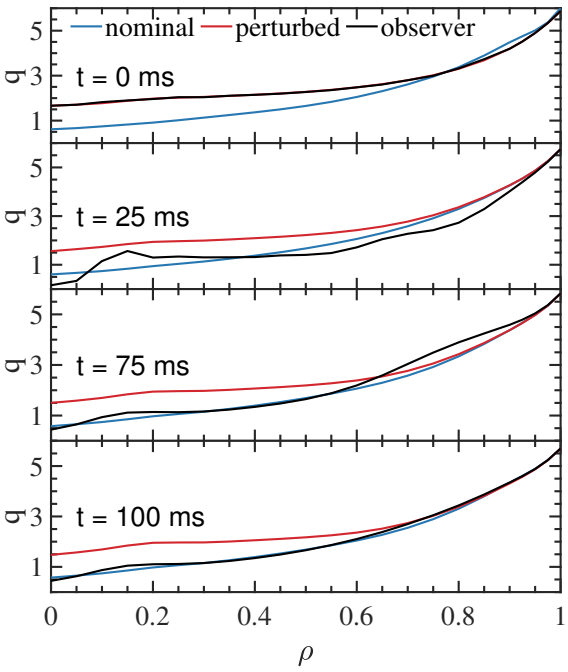

Figure 3.2: q-profile for the reference (—) and perturbed (—) simulation, as well as the q-profile resulting from the observer (—). The model of the observer is the perturbed simulation, input measurements are the noisy polarisation angles.

The observer corrects the perturbed q-profile to closely approximate the nominal case. The difference in q for each time step between the nominal case and the observer/perturbed case is calculated using the standard deviation figure of merit [26, 27]

$$\sigma(t) = \sqrt{\int_{\rho=0}^{1} d\rho (q_{\mathrm{obs,pert}} - q_{\mathrm{nom}})^2} / \sqrt{\int_{\rho=0}^{1} d\rho q_{nom}^2}. \tag{3.1}$$

Averaged over all times $t > 75$ ms, $\overline{\sigma}^{\mathrm{nom|obs}}_{t>75\ \mathrm{ms}} = 0.02$ between the nominal and observer simulation, compared to $\overline{\sigma}^{\mathrm{nom|pert}}_{t>75\ \mathrm{ms}} = 0.19$ between the nominal and perturbed case.

The convergence time depends strongly on the choice of the covariance matrix, which is used to tune the EKF. To illustrate the influence of the model covariance, figure 3.3 shows the innovation sequence for varying σ_J, the value of the diagonal elements of the model covariance matrix Q_k (see equation 2.5). With decreasing covariance an increase in convergence time is observed. Tuning of the covariance (matrix) is crucial for the operation of the EKF.

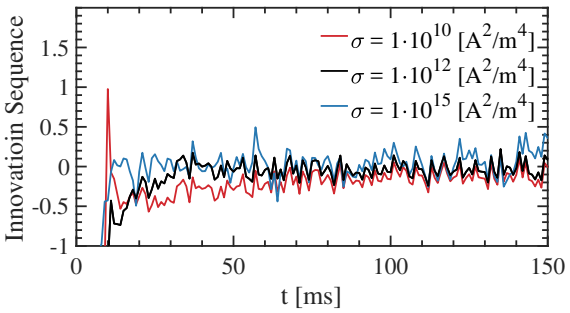

Figure 3.3: The convergence of the EKF, measured by the innovation sequence $\mathfrak{I}$, can be tuned by the covariance σ_J.

3.2 q-profile reconstruction of AUG discharge

After the initial verification using synthetic measurements, the q-profile of a full AUG discharge is reconstructed using the MSE observer. A shot with low noise MSE signals is analysed, for which a reference equilibria (reconstructed by MSE constrained IDE [11]) is available. IDE is a GS solver, which, apart from being constrained by the measurements, also evolves the poloidal flux diffusion equation in-between consecutive equilibria reconstructions. The evolved current density profile is used to constrain the next equilibrium solution. The goal of this analysis is to obtain a q-profile, filtered by the EKF, which can be compared with the IDE analysis. For the analysis, RAPTOR's heat transport model, non-inductive current density deposition profiles from ECRH and NBI as well as the non-inductive driven currents have been tuned to approximate IDE estimates. The density profiles are fixed to match IDE. A comparison between IDE and the RAPTOR simulation without the EKF is shown in figure 3.4.

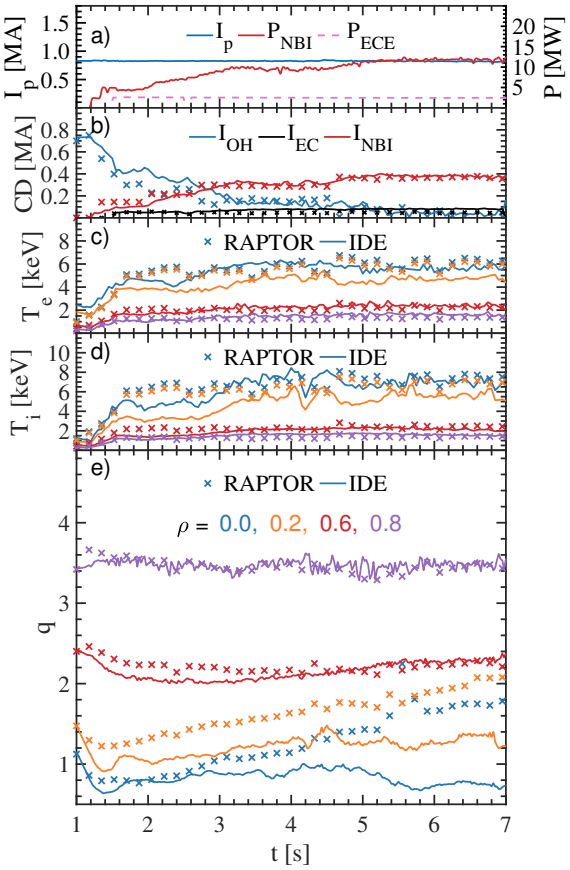

Figure 3.4: Comparison of IDE analysis and RAPTOR simulation without MSE constraint of AUG shot *#33134*: a) Plasma current and aux. power. b) Current sources from IDE (solid) and RAPTOR (dashed). c), d): Electron and ion temperature at different ρ. e) q-value evolution at different ρ. Temperature and q-values are plotted for $\rho = 0, 0.2, 0.6, 0.8$.

The MSE observer is run with the same RAPTOR configuration used to create figure 3.4 and the measured polarisation angles of shot *#33134*. The goal of the analysis is to obtain a q-profile matching the IDE analysis. The safety factor evolution of the MSE observer is shown in figure 3.5. The observer is active between 1.2 s − 7 s, the time during which MSE measurements are available.

The q-profile evolution estimated by the MSE observer is in good agreement with the IDE reference. Only in the vicinity of the magnetic axis, where the difference between the pure RAPTOR simulation and IDE is highest, a deviation from the IDE reference is notable. At the plasma edge,

a match in q between RAPTOR and IDE is guaranteed by the boundary conditions.

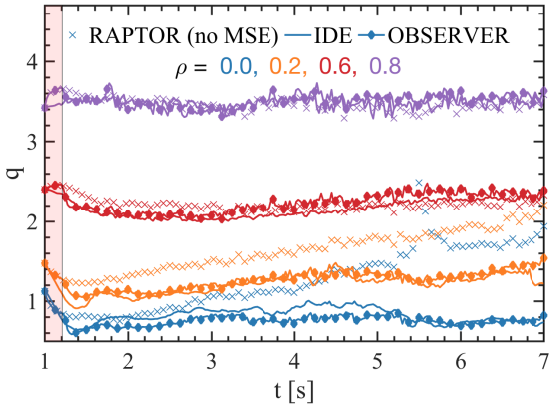

Figure 3.5: q-profile evolution at $\rho = 0$, 0.2, 0.6, 0.8 (bottom to top). Compared are three cases: RAPTOR without MSE, the reference IDE solution and the observer result. The times where the observer is inactive are shaded in red, here no MSE measurements are available. The RAPTOR time resolution is 5ms; every 35th time step is plotted for improved visibility.

The q-profiles are compared in figure 3.6 at four times. The q-values in the vicinity of the magnetic axis differ by $\Delta q \approx 1$ between the RAPTOR simulation without MSE and IDE. The MSE observer corrects the q-profile significantly. To compare the correction, the standard deviation figure of merit (see equation 3.1) is used again. Since the observer only corrects the q-profile in the plasma centre, the integral in equation 3.1 is evaluated like $\int_{\rho=0}^{0.7}$. As it was previously done, the resulting $\sigma(t)$ is averaged over all times. We find $\overline{\sigma}_{\forall t}^{\mathrm{OBS|IDE}} = 0.05$ (difference between observer and IDE reference), compared to $\overline{\sigma}_{\forall t}^{\mathrm{RAP|IDE}} = 0.19$ (difference between RAPTOR without MSE and IDE reference). For larger values of ρ, no MSE channels are available and the observer result matches the RAPTOR simulation without MSE.

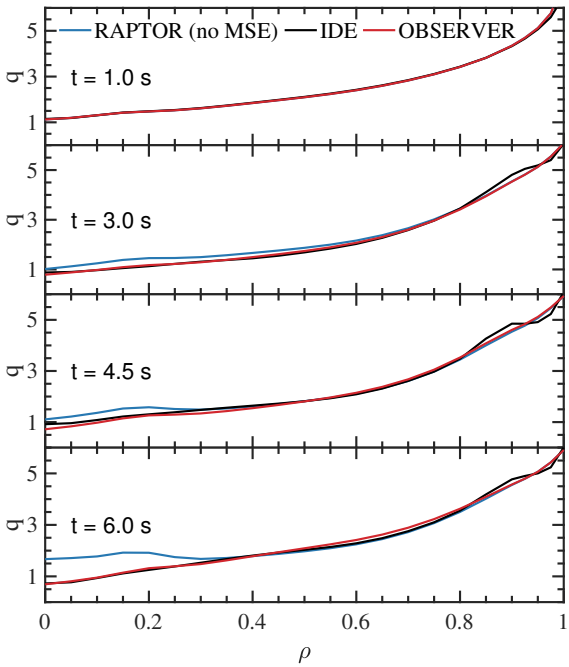

Figure 3.6: q-profile comparison between the nominal simulation (—), IDE (—) and MSE observer (—). Due to the high number of constraints, IDE is able to resolve the plasma edge more accuratetely than RAPTOR, leading to a accurate calculation of the bootstrap current at the edge and the divergence of q for $\rho > 0.8$.

Observer behaviour at signal loss

Lastly, the behaviour of the MSE observer after the loss of the MSE signal is analysed. The previous scenario is repeated, but the MSE input to the observer is cut at $t = 5$ s. The resulting time evolution of q is shown in figure 3.7. Immediately after the loss of the measurement signals, the q-profile of the observer begins to converge towards the nonconstrained case.

An advantage of using the MSE observer is the constant availability of polarisation angles which can be passed to a (real-time) Grad-Shafranov solver. In the worst case, i.e. no valid measurements are available, the q-profile is predicted based solely on the simulation model, whose information of the transport in the plasma can greatly enhance the equilibrium reconstruction. In other words: with the approach described in this article almost any GS solver can easily be constrained by the evolution of the poloidal flux calculated by RAPTOR.

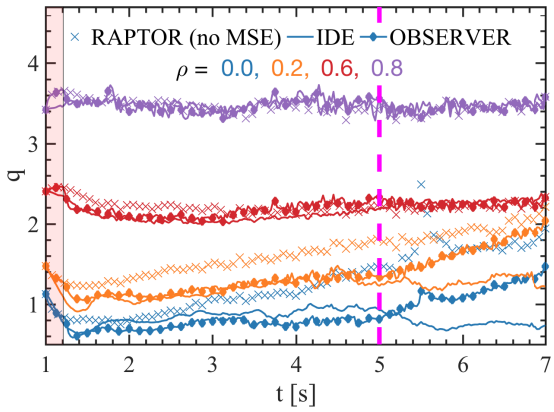

Figure 3.7: q-profile evolution at $\rho = 0,\ 0.2,\ 0.6,\ 0.8$ (bottom to top). At $t = 5$ s the measurement input to the observer is disabled and the simulation continues without being constraint by MSE measurements.

4 Conclusion & outlook

In this article we have shown that RAPTOR can be constrained by polarisation angle measurements to provide an improved estimation of the q-profile. The implemented observer is able to accurately estimate the q-profile in simulations where both the measurement and model have been perturbed. Furthermore it was shown, that in shots where reliable MSE data is available, the MSE observer constrains RAPTOR's q-profile to match reference equilibria with minimal offsets. The MSE diagnostic at ASDEX Upgrade suffers from parasitic polarised reflections from the metallic walls, which can render the diagnostic unusable in several scenarios. Due to the setup of the MSE system, which can simultaneously measure π and σ emission at the same radial location, an (real-time capable) estimate of the measurement quality is obtained. With this, the observer continuously updates the covariance matrices and it can provide estimates of the polarisation angle measurements to a GS solver in any discharge scenario, even if physical measurements are unavailable.

While the work presented here uses the CHEASE equilibrium code, which is fixed-boundary solver and not capable to run in real-time, this approach can readily be ported to a real-time capable equilibrium code such as LIUQE [28] or JANET [29]. Then, instead of using RAPTOR's q-profile, the filtered polarisation angles can be used to constrain the q-profile of the equilibrium reconstruction. In principle, this allows any Grad-Shafranov solver to be constrained by the current diffusion, heat, and particle transport between consecutive equilibria reconstruction by coupling it to RAPTOR via a virtual MSE diagnostic. The only requirement is that the GS solver can be constrained by MSE measurements.
In the future we plan to implement the observer in AUG's real-time control system, where the RAPTOR code is already implemented and a real-time capable MSE diagnostic is installed and the real-time equilibrium reconstruction code JANET are readily available.

Acknowledgement

This work has been carried out within the framework of the EUROfusion Consortium and has received funding from the Euratom research and training programme 2014-2018 under grant agree-

ment No 633053. The views and opinions expressed herein do not necessarily reflect those of the European Commission

References

[1]F. Felici, O. Sauter, S. Coda, B. Duval, T. Goodman, J.-M. Moret, and J. Paley, "Real-time physics-model-based simulation of the current density profile in tokamak plasmas", Nucl. Fusion **51**, 083052 (2011).

[2]J. P. Freidberg, *Plasma Physics and Fusion Energy*, 1st ed. (Cambridge University Press, New York, 2007).

[3]V. Mukhovatov, and V. D. Shafranov, "Plasma equilibrium in a Tokamak", Nucl. Fusion **11** (1971).

[4]L. L. Lao, J. R. Ferron, R. J. Groebner, W. Howl, H. S. John, E. J. Strait, and T. S. Taylor, "Equilibrium analysis of current profiles in tokamaks", Nucl. Fusion **30**, 1035 (1990).

[5]F. M. Levinton, R. J. Fonck, G. M. Gammel, R. Kaita, H. W. Kugel, E. T. Powell, and D. W. Roberts, "Magnetic Field Pitch-Angle Measurements in the PBX-M Tokamak Using the Motional Stark Effeect", Phys. Rev. Lett. **63**, 2060–2063 (1989).

[6]J. Blum, C. Boulbe, and B. Faugeras, "Reconstruction of the equilibrium of the plasma in a Tokamak and identification of the current density profile in real time", J. Comput. Phys. **231**, 960–980 (2012).

[7]J. Ko, "Sensitivity of magnetic field-line pitch angle measurements to sawtooth events in tokamaks", Rev. Sci. Instrum. **87**, 11E541 (2016).

[8]M. C. C. Messmer, J. Ko, J. Chung, M. H. Woo, K.-D. Lee, and R. J. E. Jaspers, "Evolution of the central safety factor during stabilized sawtooth instabilities at KSTAR", Nucl. Fusion **58**, 016030 (2018).

[9]F. L. Hinton, and R. D. Hazeltine, "Theory of Plasma Transport in Toroidal Confinements Systems", Rev. Mod. Phys. **48**, 239–308 (1976).

[10]R. Fischer, J. Hobirk, L. Barrera, A. Bock, A. Burckhart, I. Classen, M. Dunne, J. C. Fuchs, L. Giannone, K. Lackner, P. J. Mccarthy, E. Poli, R. Preuss, M. Rampp, S. K. Rathgeber, M. Reich, B. Sieglin, W. Suttrop, E. Wolfrum, and ASDEX Upgrade Team, "Magnetic equilibrium reconstruction using geometric information from temperature measurements at ASDEX Upgrade", in Proc. 40th eps conf. plasma phys. Edited by V. Naulin, (2013), P2.139.

[11]R. Fischer, A. Bock, M. Dunne, J. C. Fuchs, L. Giannone, K. Lackner, P. J. McCarthy, E. Poli, R. Preuss, M. Rampp, M. Schubert, J. Stober, W. Suttrop, G. Tardini, and M. Weiland, "Coupling of the flux diffusion equation with the equilibrium reconstruction at ASDEX Upgrade", Fusion Sci. Technol. **69**, 526–536 (2016).

[12]F. Felici, J. Citrin, A. A. Teplukhina, J. Redondo, C. Bourdelle, F. Imbeaux, O. Sauter, J. contributors, and EUROfusion MST1 Team, "Real-time-capable prediction of temperature and density profiles in a tokamak using RAPTOR and a first-principle-based transport model", Nucl. Fusion, forthcoming, (2018).

[13]F. Felici, O. Sauter, M. R. De Baar, S. Coda, B. Duval, T. Goodman, G. Hommen, J.-M. Moret, R. Voorhoeve, and M. Steinbuch, "Real-time Model-based Reconstruction and Control of Tokamak Plasma Profiles", in Iaea conf. 2012 (2012), EX/P3–12.

[14]H. Lütjens, A. Bondeson, and O. Sauter, "The CHEASE code for toroidal MHD equilibria", Comput. Phys. Commun. **97**, 219–260 (1996).

[15]D. Simon, *Optimal State Estimation*, 1st ed. (John Wiley & Sons, Inc, Hoboken, New Jersey, USA, 2006).

[16]F. Felici, M. D. Baar, and M. Steinbuch, "A dynamic state observer for real-time reconstruction of the tokamak plasma profile state and disturbances", in Am. control conf. (2014), pp. 4816–4823.

[17]A. A. Teplukhina, O. Sauter, F. Felici, A. Merle, D. Kim, TCV Team, ASDEX Upgrade Team, and EUROfusion MST1 Team, "Simulation of profile evolution from ramp-up to ramp-down and optimization of tokamak plasma termination with the RAPTOR code", Plasma Phys. Control. Fusion **59**, 124004 (2017).

[18]J. Van Dongen, F. Felici, G. M. D. Hogeweij, P. Geelen, and E. Maljaars, "Numerical optimization of actuator trajectories for ITER hybrid scenario profile evolution", Plasma Phys. Control. Fusion **56** (2014) 10.1088/0741-3335/56/12/125008.

[19]R. Reimer, A. Dinklage, J. Geiger, J. Hobirk, M. Reich, R. Wolf, ASDEX Upgrade, and Wendelstein 7-X Teams, "Motional Stark effect spectra simulations for Wendelstein 7-X", Contrib. to Plasma Phys. **50**, 731–735 (2010).

[20]R. C. Wolf, A. Bock, O. P. Ford, R. Reimer, A. Burckhart, A. Dinklage, J. Hobirk, J. Howard, M. Reich, and J. Stober, "Motional Stark Effect measurements of the local magnetic field in high temperature fusion plasmas", J. Instrum. **10**, P10008 (2015).

[21]A. Bock, E. Fable, R. Fischer, M. Reich, D. Rittich, J. Stober, M. Bernert, A. Burckhart, H. Doerk, M. Dunne, B. Geiger, L. Giannone, V. Igochine, A. Kappatou, R. McDermott, A. Mlynek, T. Odstrčil, G. Tardini, and H. Zohm, "Non-inductive improved H-mode operation at ASDEX Upgrade", Nucl. Fusion **57** (2017) 10.1088/1741-4326/aa8967.

[22]R. T. Mumgaard, S. D. Scott, and M. Khoury, "The multi-spectral line-polarization MSE system on Alcator C-Mod", Rev. Sci. Instrum. **87**, 87–90 (2016).

[23]B. W. Rice, K. H. Burrell, and L. L. Lao, "Effect of plasma radial electric field on motional Stark effect measurements and equilibrium reconstruction", Nucl. Fusion **37**, 517–522 (1997).

[24]B. W. Rice, D. G. Nilson, K. H. Burrell, and L. L. Lao, "Simultaneous measurement of q and Er profiles using the motional Stark effect in high-performance DIII-D plasmas", Rev. Sci. Instrum. **70**, 815 (1999).

[25]L. Blondel, and O. Sauter, "Axisymmetric Tokamak Equilibria computed with a Predefined Safety Factor Profile as CHEASE input", Master project (EPFL, 2016).

[26]C. Holland, "Validation metrics for turbulent plasma transport", Phys. Plasmas **23** (2016) 10.1063/1.4954151.

[27]"ITER Physics Expert Group on Confinement and Transport et al", Nucl. Fusion **39**, 2175 (1999).

[28]J. M. Moret, B. P. Duval, H. B. Le, S. Coda, F. Felici, and H. Reimerdes, "Tokamak equilibrium reconstruction code LIUQE and its real time implementation", Fusion Eng. Des. **91**, 1–15 (2015).

[29]L. Giannone, M. Reich, M. Maraschek, E. Poli, C. Rapson, L. Barrera, R. McDermott, A. Mlynek, Q. Ruan, W. Treutterer, L. Wenzel, A. Bock, G. Conway, R. Fischer, J. C. Fuchs, K. Lackner, P. J. McCarthy, R. Preuss, M. Rampp, K. H. Schuhbeck, J. Stober, H. Zohm, and ASDEX Upgrade Team, "A data acquisition system for real-time magnetic equilibrium reconstruction on ASDEX Upgrade and its application to NTM stabilization experiments", Fusion Eng. Des. **88**, 3299–3311 (2013).